Computational Mechanics 24 (1999) 258–267 © Springer-Verlag 1999

An efficient algorithm for propagating fluid-driven fractures

P. Papanastasiou

Abstract This paper presents an efficient finite element algorithm for propagating fluid-driven fractures in pressure sensitive geomaterials. Fluid flow in the fracture is modelled by lubrication theory. Rock deformation is assumed to be elastoplastic and dilatent. A cohesive model based on the softening behaviour of rocks is employed as the propagation criterion. A special continuation method based on the volume of injected fluid in the fracture is used for direct coupling of the fluid-flow with rock deformation and for driving the solution during propagation. Sample results are provided for the problem of hydraulic fracturing to demonstrate the efficiency of the proposed algorithm.

1 Introduction

The problem of a fluid-driven fracture has attracted many contributions since the early fifties (Kristianovitch and Zheltov, 1955; Geertsma and DeKlerk, 1969). Interest in such studies rises mainly from hydraulic fracturing, a technique for stimulating hydrocarbon reservoirs but also from other applications such as magma driven fracture (Spence and Turcotte, 1985). With hydraulic fracturing, a wellbore interval is pressurized with viscous fluid at high pumping rates to initiate and propagate a tensile fracture. Once the fracture is created, it is packed with proppant (material like sand) to prevent closure after the hydraulic pressure is released. The created propped fracture provides a highly conductive path for the flow of hydrocarbons towards the well. New applications of hydraulic fracturing have been recently found in geotechnical engineering for ground reinforcement, in petroleum engineering for re-injection of drilling cuttings and in environmental engineering for solids waste disposal. Modelling the propagation of hydraulic fractures is usually carried out prior to fracturing in order to optimize the treatment for maximum efficiency. Optimization is carried out using models that incorporate principles of fluid mechanics, elasticity, and fracture mechanics. Parameters which are optimized include the fracture length and width, fluid design and pumping schedule.

Received 5 February 1999

P. Papanastasiou
Schlumberger Cambridge Research,
High Cross, Madingley Road,
Cambridge CB3 0EL, England

In practice, a lot of attention is focussed on the prediction of wellbore pressure; wellbore pressure is normally measured during the treatment and is usually the only parameter available to evaluate the operation. Classical hydraulic fracturing simulators often underestimate the down-hole pressures which are measured in field operations. A recent world-wide survey on net-pressures (difference between fracturing pressure and far-field confining stress) indicated that net-pressures encountered in the field are 50% to 100% higher than the net-pressures predicted by the conventional hydraulic fracturing simulators (van Dam et al., 1997). The occurrence of high net pressures triggered a series of dedicated research studies and several hypotheses have been proposed to explain the discrepancy between model predictions and field measurements. Among them, the most consistent with observations are (1) high friction losses in constrictions within a fracture and (2) effective fracture toughness effects (e.g. due to micro-cracking or plasticity in the process zone).

According to the first hypothesis, the observed high net pressure is related to a sharp drop of fluid-pressure and the existence of a dry region near the crack-tip (Johnson and Cleary, 1991). Earlier models often ignored the existence of a fracturing fluid front and arbitrarily assigned (sometimes wrongly) a pressure condition at an arbitrary location. Fluid front tracking, however, involves an unknown position and requires iteration in the numerical procedure. This cumbersome process fuelled the motivation for understanding first the nature of the solution in the vicinity of the crack tip (Sharp and Spence, 1985) and for developing later a 'crack tip element' (Desroches et al., 1994; Carbonell and Detournay, 1999). The tip region behaviour is an important aspect of the problem and a near-tip analytical solution could be used either to obtain a complete analytical model for fractures with plane strain (Garagash and Detournay, 1999) and penny-shape (Savitski and Detournay, 1999) geometries or to provide tip region boundary conditions in a numerical model of the complex geometry problem (Carter et al., 1999). A thorough discussion on these studies can be found in Detournay (1999).

The second hypothesis implies that the non-linear deformation of the rock might have a strong influence in hydraulic fracturing. This hypothesis is strongly supported by the recent survey on the net pressures which revealed that the difference between model predictions and field measurements was consistently higher in weak formations (van Dam et al., 1997). In addition, it is important to mention that in the last decade fracture design has chan-

ged from long fractures to shorter and wider fractures. The need for modelling the non-linear rock behaviour could be justified following two avenues. The first avenue suggests that the non-linear rock behaviour will induce a pressure profile near the crack tip that is quite different from that predicted by linear elasticity. This could affect the complete pressure response (Barr, 1991) . One can include in this approach the possibility of fracture multi-branching which was mainly based on observations from a field experiment (GRI, 1991). However, Germanovich et al. (1988) recently showed that propagation of multiple fractures does not necessarily cause a significant increase in required net pressure. The second avenue states that the energy required to create new rock surface(s) dominates the pressure response. This energy must be much higher than the free surface energy measured in small scale laboratory experiments and the influence of large scale heterogeneities or large scale plasticity could be introduced. In this approach, the viscous loss could be neglected and the pressure in the crack could be assumed to be uniform (Shlyapobersky, 1985).

In an attempt to explain the observed high net pressures, we developed an elastoplastic hydraulic fracturing model. Conclusions derived from an analytical solution for elastic materials (Desroches et al., 1994) and from preliminary computations, showed that the stress and deformation fields around the fracture tip depend strongly on the fluid-flow in the fracture. It is therefore essential to solve the problem fully coupled, although it becomes highly non-linear. This paper concentrates on the numerical aspects of the involved processes with particular emphasis on the solution algorithm used for direct coupling of the fluid-flow with rock deformation during propagation. The proposed model has been tried successfully in a series of studies which are related to the influence of plastic deformation in hydraulic fracturing (Papanastasiou and Thiercelin, 1993; Papanastasiou, 1997a; Papanastasiou, 1999a). We found that plastic yielding near the tip of a propagating fracture provides an effective shielding, resulting in an increase of the rock effective fracture toughness by more than an order of magnitude (Papanastasiou, 1999a). Higher pressure is needed for propagating an elasto-plastic fracture than an elastic fracture and the created elasto-plastic fracture is shorter and wider than the elastic fracture of the same volume (Papanastasiou, 1997a).

The paper is organized as follows: firstly we describe in Sect. 2 the involved processes in the model which are the fluid-flow, rock deformation and fracture propagation. Fluid flow in the fracture is modelled by lubrication theory. Rock deformation is assumed to behave like an elastoplastic and dilatant Mohr-Coulomb solid. The propagation criterion is based on the softening behaviour of rocks. In Sect. 3, we present a special continuation method based on the volume of injected fluid in the fracture which is used for direct coupling of the fluid-flow with rock deformation and for controlling the solution during propagation and closure. In Sect. 4, we present sample results for propagating and receding elastic and elastoplastic hydraulic fractures to demonstrate the efficiency of the developed algorithm.

2
Model description

The developed model is based on a plane strain fracture geometry (Fig. 1). This is the most appropriate geometry for short fractures with fracture height relatively large compared to the fracture length. In addition, this geometry is appropriate for examining tip effects since the deformation near the tip of any arbitrary shape fracture becomes planar. We note, in parenthesis, that fractures initiated either from perforations or directly from the wellbore are initially aligned with the near-wellbore stress field, but quickly reorient themselves to propagate in the preferential plane which is perpendicular to the far-field minimum in situ stress. The length-scale where fracture re-orientation takes place is much smaller than the fracture length so it can easily be ignored. In this study, we simply assume that the fracture propagates perpendicular to the minimum in situ stress remaining planar.

Describing the model using Fig. 1, the pumping viscous fluid pressurizes the fracture surfaces which deform. Depending on formation properties, in situ stresses and pumping parameters, the fluid may not necessarily reach the fracture tip thus allowing for the possibility of a dry zone (fluid lag) near the fracture tip. Due to high stress concentration near the tip region, plastic deformation may take place resulting in stress redistribution and tip shielding. With increasing pressurization, critical stress conditions ahead of the tip will be reached splitting the formation and driving fracture propagation. Thus, there is a strong coupling between moving fluid, rock deformation and fracture propagation. In summary, the main physical processes which govern hydraulic fracturing in a weak formation are (1) viscous fluid flow in the fracture, (2) elastoplastic deformation caused by the stress concentration, (3) fracture propagation and (4) fluid leak-off from the fracture into the formation. The last process is not taken into consideration here assuming that in practice fluid leak-off can be controlled by fluid additives.

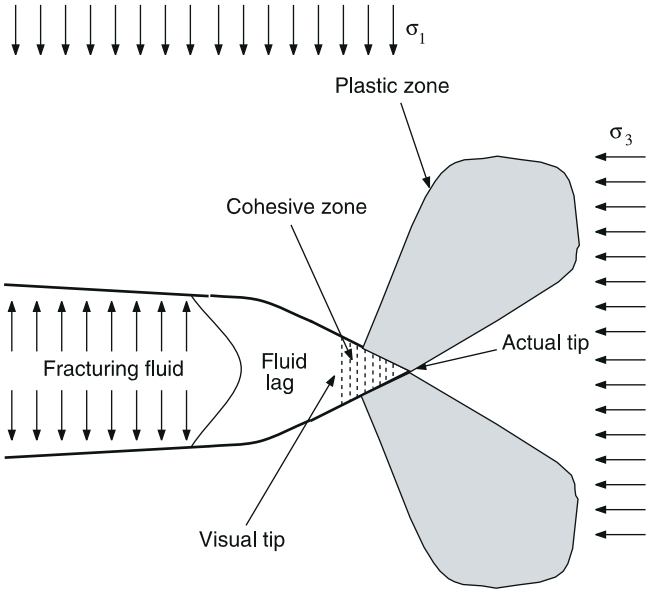

Fig. 1. Geometry for a plane strain hydraulic fracture

2.1 Fluid-flow

Most of the fluids that are used for hydraulic fracturing are power-law fluids with a shear-thinning behaviour, meaning that the viscosity decreases with increasing shear-strain rate. For simplicity, we assume in this study that the fracturing fluid is an incompressible, uniform, linear (Newtonian) viscous fluid. A Newtonian fluid has a parabolic profile when it flows between parallel plates with shear rates of zero in the middle of the profile and higher towards the sides. Fluid-flow will be approximated here using an average fluid velocity, v, and an effective channel viscosity, $\bar{\mu}$.

The first fluid-flow equation is derived from the continuity equation which imposes conservation of mass in one dimensional flow

$$\frac{\partial w}{\partial t} + \frac{\partial q}{\partial x} = 0 \quad , \tag{1}$$

where w is the local fracture width and q is the local flow rate. Equation (1) ignores any leak-off from the fracture surface into the rock formation.

A second equation is derived from conservation of momentum. For a fluid-flow between parallel plates the lubrication equation, which relates the pressure gradient to the fracture width for a Newtonian fluid of viscosity μ degenerates to

$$q = vw = -\frac{w^3}{12\mu}\frac{\partial p}{\partial x} \quad , \tag{2}$$

where p denotes the fluid pressure in the fracture. The effective channel flow viscosity $\bar{\mu}$ is introduced because it appears in the denominator of (2) for the average fluid velocity and it is directly related to the fluid viscosity, $\bar{\mu} = 12\mu$.

The fluid-flow Eqs. (1) and (2) are supplemented with a first boundary condition for a given flow rate at the wellbore

$$q(0) = q_0 \quad . \tag{3}$$

As mentioned earlier, the fluid may not necessarily reach the fracture tip allowing for the possibility of a fluid lag near the tip. In such a case the existence of a fluid-lag provides a second boundary condition. The pressure in the fluid-lag region can take either a maximum value equal to the pore-pressure when the fracture propagates slowly in a high permeability rock or it can be zero if the fracture propagates relatively fast in a low permeability rock. In this study we will assume the latter case since fluid infiltration and diffusion from the fracture into the rock and vise-versa are ignored. Therefore, a second boundary condition is defined at the fluid-front

$$p(l) = 0 \quad . \tag{4}$$

Equation (2) can be used to determine the pressure profile along the fracture from the local width, w, and local flow rate, q, starting the integration from a reference pressure. According to (2), the pressure gradient is very sensitive to fracture width:

$$\frac{\partial p}{\partial x} = -q\bar{\mu}\frac{1}{w^3} \quad . \tag{5}$$

Therefore, the largest part of the pressure drop takes place within a small area near the tip region where the width varies most, approaching zero value. In the numerical models due to the steep gradient at the fluid-front region, an attempt to start the pressure integration from the fluid-front position using (4) and (5) becomes a cumbersome procedure because small variation in the fracture width during the iteration cycle results in pressure overshooting. As an alternative solution, we propose in Sect. 3 a pressure integration scheme which starts from the wellbore. The required reference pressure at the wellbore is determined indirectly from the condition that the fracture must be at propagation state. The position of the fluid-lag is determined from the mass balance equation (1) and the boundary condition (4).

2.2 Inelastic rock deformation

In weak rocks, large inelastic deformation is expected to take place in the area near the crack tip due to excessive stress concentration. In such a case one should use plasticity theory which properly describes the irreversible deformation. When the fracture propagates the plastic zones unload elastically behind the advancing crack and the new area near the current tip deforms plastically. In summary, the rock mass remote from the fracture may deform elastically, whereas the area near the body of the fracture is initially elastic but then deforms plastically and finally unloads elastically after the fracture tip has advanced. Under such conditions, the plasticity model must be capable of dealing with non-proportional loading. Such capabilities are provided, of course, by an incremental flow theory of plasticity and finite element analysis.

Among the different yield criteria, the Mohr-Coulomb model adequately describes the pressure-sensitive behaviour of rocks which exhibit dilatency when sheared. Unlike most cases of classical fracture mechanics, the remote stress field in the hydraulic fracturing problem is compressive, due to the presence of the in situ stresses. In such a case the use of Mohr-Coulomb yield criterion, which is usually employed in cases of compressive stresses, is fully justified. The tensile failure along the propagation line is modelled in the next section by a cohesive-type model. In a simple form, the Mohr-Coulomb yield criterion can be expressed in terms of maximum and minimum principal stresses, σ_1 and σ_3, respectively, (compression is negative)

$$\sigma_e = \sigma_1\frac{1+\sin\phi}{1-\sin\phi} - \sigma_3 \quad , \tag{6}$$

where ϕ is the friction angle and σ_e is the equivalent stress which is related to the cohesion c via

$$\sigma_e = 2c\frac{\cos\phi}{1-\sin\phi} \quad . \tag{7}$$

Post yield strengthening with deformation can be modelled using a cohesion hardening model. According to this model the equivalent stress, σ_e, increases with the accumulated equivalent plastic strain, ϵ^p,

$$\sigma_e = \sigma_e^0 + h\epsilon^p \quad , \tag{8}$$

where σ_e^0 is the value of equivalent stress at initial yield. The linear hardening plasticity modulus h has been derived in Papanastasiou (1997) from the loading and unloading moduli as measured in a uniaxial compression test.

$$h = \frac{E_{\text{loading}}}{1 - E_{\text{loading}}/E_{\text{unloading}}} \quad . \tag{9}$$

In the flow theory of plasticity the strain increment $\mathrm{d}\epsilon_{ij}$ is decomposed into an elastic $\mathrm{d}\epsilon_{ij}^e$ and a plastic part $\mathrm{d}\epsilon_{ij}^p$

$$\mathrm{d}\epsilon_{ij} = \mathrm{d}\epsilon_{ij}^e + \mathrm{d}\epsilon_{ij}^p \quad . \tag{10}$$

The elastic strain increment $\mathrm{d}\epsilon_{ij}^e$ can be obtained from Hooke's law. The plastic strain increments, $\mathrm{d}\epsilon_{ij}^p$, are generated when the yield surface is reached and can be generally expressed by a non-associated flow rule in the form

$$\mathrm{d}\epsilon_{ij}^p = \mathrm{d}\lambda \frac{\partial Q}{\partial \sigma_{ij}} \quad , \tag{11}$$

where Q is the plastic potential and the scalar function $\mathrm{d}\lambda$ is the so called plastic multiplier. The plastic potential Q can have a similar form to yield surface σ_e, if in Eq. (6) the dilation angle ψ replaces the friction angle ϕ. This allows non-associated plasticity to be dealt with, and associated rules to be obtained as a special case, by making $\psi = \phi$ or $Q = \sigma_e$.

As mentioned before, the yield surface and plastic potential are generally functions of stresses and the hardening parameter ϵ^p (a scalar). The hardening parameter ϵ^p is calculated from the principle of plastic power equivalence (Papanastasiou and Durban, 1997),

$$\sigma_e \mathrm{d}\epsilon^p = \sigma_{ij} \mathrm{d}_{ij}^p \quad . \tag{12}$$

In general, weak rocks obey a non-linear yield criterion and exhibit non-associative behaviour. Experimental results from triaxial compression tests show (a) that the dilation angle increases slightly with increasing plastic strain when low confining pressures are used but remains approximately constant in samples under high confining pressure and (b) the value of dilation angle is a strong function of the confining pressure. In tests with low confining pressure the measured dilation angle is greater than the friction angle but decreases rapidly with increasing confining pressure, eventually becoming negative. This indicates compaction at very high confining pressure. In hydraulic fracturing, compaction is excluded because the initial in-situ mean pressure near the crack tip decreases during propagation. Furthermore, earlier computations by Papanastasiou and Thiercelin (1993) showed that the non-associative solution (e.g. zero dilation) was bounded by the associative solution and the elastic solution.

2.3 Propagation criterion

The most robust propagation criterion currently available in non-linear mechanics is based on constitutive modelling of the cohesive zone (Barenblatt, 1962). The cohesive zone is the region ahead of crack tip that is characterized by micro-cracking and interlocking along a portion of the crack (Fig. 1). According to Labuz et al. (1985) and Bazant (1986) the main fracture is formed by inter-connection of these micro-cracks. The cohesive model implies that normal stress continues to be transferred across a discontinuity which may or may not be visible (Fig. 2). This stress is determined from the softening stress-displacement relation that various rocks exhibit in the post-peak regime of calibration tests. In this separation process, the restraining stress, σ is a function of opening displacement δ which falls off to zero at a critical opening displacement δ_c and the actual crack propagates (Fig. 2). It is also assumed that the cohesive zone localizes, due to the softening behaviour, into a narrow band ahead of the true crack tip. The last assumption is very convenient for finite element analysis, where the softening behaviour is modelled by interface elements lying in the direction of crack growth, ahead of the true crack tip (Hillerborg et al., 1976).

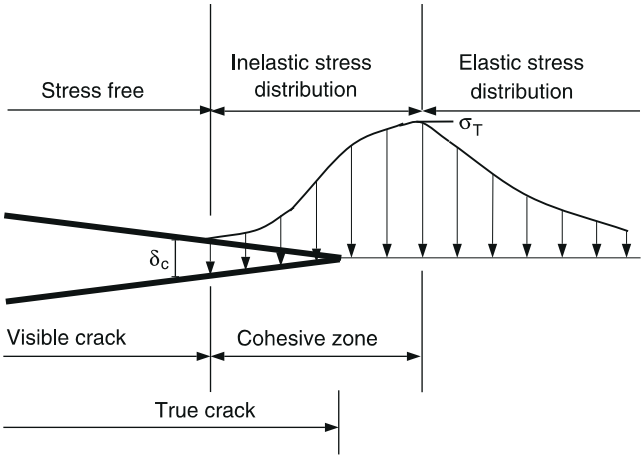

Fig. 2. Representation of the fracturing process of rock

The constitutive behaviour of interface elements can be defined by the stress-displacement curve which is usually derived from a displacement control uniaxial tensile test. Because of the confinement by the in situ stresses in the problem of hydraulic fracturing, the stress path ahead of the fracture tip has more similarities with the triaxial extension test rather than with the direct tensile test. Furthermore, a direct tensile test is difficult to perform in weak or poorly consolidated sandstones. Due to the lack of available data, and in order to keep the number of input parameters minimum, a linear softening material was assumed (Fig. 3). The area under the stress-displacement curve, (δ) equals the strain energy release rate G_{IC} when the size of the cohesive zone is small compared to the crack length. For elastic solids the strain energy release rate, G_{IC} is related to rock fracture toughness, K_{IC} via (Kanninen and Popelar, 1985):

$$K_{IC}^2 = \frac{G_{IC} E}{1 - \nu^2} \quad , \tag{13}$$

where E is the Young's modulus and ν is the Poisson ratio. The fracture toughness, K_{IC}, is defined as a material parameter for elastic solids and can be calculated in a lab experiment as long as no plastic yielding takes place around the tip. If one assumes reasonable values for the

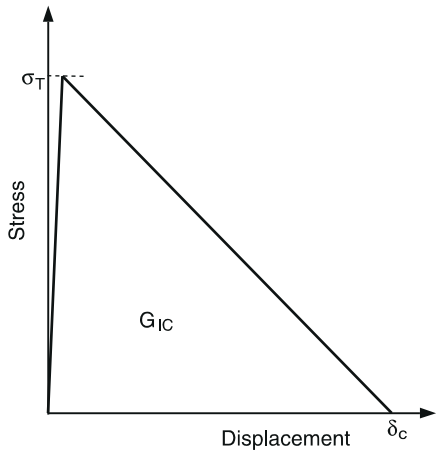

Fig. 3. Constitutive model for the cohesive zone

rock fracture toughness K_{IC} and the uniaxial tensile strength of the rock (approximately 8 to 10 times less than the uniaxial compressive strength, $\sigma_c = 10\sigma_T$) the stress-displacement relation, $\sigma(\delta)$, is uniquely determined from equation:

$$\sigma = \sigma_T(1 - \delta/\delta_c) \tag{14}$$

where σ_T is the uniaxial tensile strength of the rock and δ_c is the critical opening displacement at which σ falls off to zero. The value of δ_c, is given by,

$$\delta_c = \frac{2K_{IC}^2(1-\nu^2)}{E\sigma_T} \tag{15}$$

In this study a two-dimensional, isoparametric, 6-node interface element was employed. A consistent isoparametric formulation permits modelling of curved crack surfaces and provides an element that is compatible with the 8-node quadratic displacement finite elements that are used to discretized the internal domain.

2.4
Initial solution

The numerical algorithm requires initial conditions to be specified at $t = 0$ for the initial fracture length $\ell(0)$, width profile $w(x,0)$ and fluid pressure $p(x,0)$. In setting these initial conditions, the analytic solution derived in Desroches et al. (1994) for an elastic material with zero fracture toughness has been used. This solution is summarized as follows:

$$p(x,0) = \sigma_1 + \left(\frac{E'\mu v}{3}\right)^{1/3}\left[\frac{6\sqrt{2}}{\pi}\frac{1}{\ell(0)^{1/3}} - \frac{1}{(\ell(0)-x)^{1/3}}\right] \tag{16}$$

$$w(x,0) = (\ell(0)-x)^{2/3}\left(\frac{\mu v}{E'}\right)^{1/3} \times \left[7.21 - 3.17\left(1 - \frac{x}{\ell(0)}\right)^{5/6}\right] \tag{17}$$

where σ_1 is the in situ stress perpendicular to the fracture axis, $E' = E/(1-\nu)^2$ is the plane strain modulus, μ is the fluid viscosity and v is the propagation velocity given in terms of flow rate q_0 by

$$v = 0.835q(0)^{3/4}\ell(0)^{-1/2}\left(\frac{E'}{\mu}\right)^{1/4} \tag{18}$$

The solution described by Eqs. (16)–(18) has been derived under the assumption of constant velocity $v = \text{const.}$ and it pertains to the near tip region. This solution has recently been extended by Carbonell and Detournay (1999) to apply to the whole of the hydraulic fracture.

The numerical model of fluid-driven fractures requires an initial fracture length which may leave its signature on propagating elastoplastic fractures since plasticity is path dependent. It has been shown in Papanastasiou (1997a), where propagations were carried out with different initial lengths, the initial fracture length had an effect on the fracture profiles in the initial fracture length interval, but, the fracture profiles were correctly calculated in the region where the fractures were propagated. In addition, we found that the elastoplastic and elastic solutions are relatively close at the first propagation step (Papanastasiou, 1997a). This observation justifies the use of the elastic analytic solution as an initial solution for the propagation of elastoplastic fractures.

3
Numerical implementation

3.1
Coupling of fluid-flow and solid deformation

The described time-dependent non-linear problem of hydraulically propagating fractures is solved coupled following an incremental/iterative procedure. Incremental analysis is employed for propagating the fracture and iterative procedure is required to bring the fluid-flow, rock deformation and fracturing processes in equilibrium at every propagation step. The in situ stresses are applied in the first propagation step along with the initial solution for the pressure in the fracture given by (16). During fracture propagation the fluid pressure in fracture, denoted by $\lambda\{P\}$ is unknown and needs to be determined. $\{P\}$ is a normalized pressure and λ is a pressure multiplier. The meaning of these terms will be explained further in the coupling of fluid-flow with the rock deformation. The governing equation, in terms of the unknown nodal incremental displacement $\{\Delta U\}$ at the $(m+1)$th propagation step, is obtained from the well known equation of non-linear finite element analysis

$$\int_\Omega [B]^{\mathrm{T}}[D^{ep}][B]\{\Delta U\}\mathrm{d}\Omega = \lambda_{m+1}\{P\} - \int_\Omega [B]^{\mathrm{T}}\{\sigma_m\}\mathrm{d}\Omega \tag{19}$$

or

$$[K]\{\Delta U\} = \{R\} \tag{20}$$

where $[K]$ is the global stiffness matrix

$$[K] = \int_\Omega [B]^{\mathrm{T}}[D^{ep}][B]\mathrm{d}\Omega \tag{21}$$

and

$$\{R\} = \lambda_{m+1}\{P\} - \int_{\Omega} [B]^{\mathrm{T}}\{\sigma_m\}\mathrm{d}\Omega \tag{22}$$

is the residual vector (or unbalanced forces) which can be visualized as additional nodal forces required to bring the assumed displacement pattern into nodal equilibrium. Thus, the nonlinear problem is stepwise linearized and the linearization error is corrected by additional equilibrium iterations. The technique of choice for solving the nonlinear equation set, is Newton's method.

During fracture propagation, the pressure at the wellbore may raise or drop therefore the pressure level can not predetermined. This problem is solved by adapting one of the several methods described in the literature for tracing the response of structures near limit points (Ramm, 1981). An elegant procedure for overcoming limit points is an indirect displacement control; this method is summarized hereafter. The increment $\{\Delta U\}^{(j)}$, in the iteration j following the i iteration, from Eq. (19) is conceived to be composed of two contributions:

$$\{\Delta U\}^{(j)} = \Delta\lambda^{(j)}\{\Delta U\}_{\mathrm{I}}^{(j)} + \{\Delta U\}_{\mathrm{II}}^{(j)} \tag{23}$$

with

$$\begin{aligned} \{\Delta U\}_{\mathrm{I}}^{(j)} &= [K^{(i)}]^{-1}\{P\} \\ \{\Delta U\}_{\mathrm{II}}^{(j)} &= [K^{(i)}]^{-1}\{R\}^{(i)} \end{aligned} \tag{24}$$

and the level of applied pressure is

$$\lambda_{m+1}^{(j)} = \lambda_{m+1}^{(i)} + \Delta\lambda^{(j)} \tag{25}$$

After computing the displacement vectors $\{\Delta U\}_{\mathrm{I}}^{(j)}$ and $\{\Delta U\}_{\mathrm{II}}^{(j)}$, the value for $\Delta\lambda^{(j)}$ is determined from some constraint equation on the displacement increments. As a constraint we will use the global mass balance equation which says that in time Δt the volume of the injected fluid in the fracture must be equal with the volume increase of the fracture occupied by fluid. Suppose that in the propagation step, $(m+1)$ we have injected in the fracture fluid of volume

$$\Delta V = q_0 \Delta t \tag{26}$$

where q_0 is from the boundary condition (3). If $\Delta V_{\mathrm{I}}^{(j)}$ and $\Delta V_{\mathrm{II}}^{(j)}$ denote the volume changes of the fracture which correspond to the displacements of fracture boundary filled with fluid, $\{\Delta U\}_{\mathrm{I}}^{(j)}$ and $\{\Delta U\}_{\mathrm{II}}^{(j)}$, respectively, then the volume increase, $\Delta V^{(j)}$ in the iteration j, is given by

$$\Delta V^{(j)} = \Delta\lambda^{(j)}\Delta V_{\mathrm{I}}^{(j)} + \Delta V_{\mathrm{II}}^{(j)} \tag{27}$$

In the first iteration we have, $\Delta V^{(1)} = \Delta V$ and (27) allows the determination of the incremental pressure multiplier

$$\Delta\lambda^{(1)} = \frac{\Delta V - \Delta V_{\mathrm{II}}^{(1)}}{\Delta V_{\mathrm{I}}^{(1)}} \tag{28}$$

In all further iteration the fracture volume is kept constant, therefore $\Delta V = 0$ and the value of $\Delta\lambda^{(j)}$ is

$$\Delta\lambda^{(j)} = -\frac{\Delta V_{\mathrm{II}}^{(j)}}{\Delta V_{\mathrm{I}}^{(j)}} \tag{29}$$

The described continuation method enables the simultaneous control of the solution during propagation and the direct coupling of fluid-flow with rock deformation. This coupling passes through the term $\lambda\{P\}$ where, as already mentioned, $\{P\}$ is the eigen-pressure vector along the fracture with unit value at wellbore and λ is the value of the pressure at wellbore and it is determined implicitly from Eqs. (25)–(29). The term $\lambda\{P\}$ gives the applied pressure along the fracture. The eigen-pressure vector $\{P\}$ is determined as follows: First we note that for internally pressurized cracks the fracture width is governed by the net-pressure. For example, the profile of an elastic crack of length L which is loaded with uniform internal pressure p_f and remote confining stress σ_1 (negative) has an elliptical shape given by

$$w = 4\frac{p_f + \sigma_1}{E'}\sqrt{L^2 - x^2} \tag{30}$$

Along this line, we found that if the eigen-pressure vector is constructed from net-pressure the algorithm results in a much faster convergence. The eigen-pressure vector $\{P\}$ is determined following a second order, $0(h^2)$, Euler integration scheme of Eq. (5). The 1-D space discretization of the fluid-flow equation is identical with the discretization of the fracture boundary. The 2nd order Euler integration starts always from the wellbore with value $P(0) = 1$ and it shoots to the side of the crack tip. The eigen-pressure at the node $(n+1)$ is calculated from

$$P^{(n+1)} = P^{(n)} - \frac{\mathrm{d}p}{\mathrm{d}x}^{(n+1/2)} \mathrm{d}x^{(n)}/(p_w + \sigma_1) \tag{31}$$

where p_w is the pressure at the wellbore in the last iteration. In the fluid-lag region the eigen-pressure is constant given by

$$P^{\mathrm{lag}} = \frac{\sigma_1}{p_w + \sigma_1} \tag{32}$$

The fluid-front position is found at the point where the fluid-pressure changes sign. In addition, the way the iterative process is conducted warranties that the fluid-front position satisfies the global mass equation. Nevertheless, post-calculation checking verified that the new fluid-front position agrees with the expected movement of the fluid-front in time increment Δt according to the average fluid-front velocity, v, predicted by (2). Depending mainly on pumping parameters (flow rate and fluid viscosity) the fluid-front may reach the cohesive zone (visual tip). In that case the fluid lag disappears and the value of fluid pressure is determined from (31).

We note that in the described continuation scheme the eigen-load changes in every iteration whereas in the continuation methods belonging to arc-length or displacement control families the loading is proportional; all load magnitudes vary with a single scalar parameter (e.g. the parameter λ). This is a result of the varying pressure from the fluid-flow in the fracture. Furthermore, if in the Eqs. (27)–(29) the change of volume of the fracture ΔV is replaced by the displacement ΔU_k of any node k, the procedure reverts to the standard displacement control method. However, we found that it is easier to control the volume of the fracture which reaches a constant rate in-

crease after the first steps of propagation. Following such a control procedure, convergence is reached faster and the fracture propagation criterion is satisfied exactly in every propagation step.

We found the displacement control approach to be more convenient method for modelling fracture closure. During closure it is assumed that there was no fluid-flow in the fracture and as a result the pressure acting along the fracture was constant. At every step the displacement of the first node of the element behind the crack-tip is fixed to the negative value of its opening. In this way, the use of contact algorithm for preventing surface overlap during closure is not required.

3.2
Finite element discretization

The calculations were carried out using the 8-node quadrilateral elements and a nine-point Gaussian integration for the internal domain. Compatible 6-node isoparametric quadratic displacement interface finite elements with zero thickness were used for modelling the fracturing process. Singular elements near the crack tip, which widely employed in elastic singularities of $1/\sqrt{r}$ type, were not employed here since plastic yielding and cohesive modelling which is employed as a fracture propagation criterion cancel the singular fields near the fracture tip. An explicit technique, similar to the Euler forward method has been employed in the integration of the stress-strain law. Convergence criterion for terminating the equilibrium iterations has been chosen the Euclidean norm of the out of balance forces not to exceed a percentage (0.01%) of the norm of the applied external load.

A meshing/remeshing scheme is employed in order to carry out longer propagations with fine mesh near the fracture tip. The meshing/remeshing scheme was based on the following steps: The sensitive area near the tip where high gradients exist was discretized using a fine mesh and the region away from the crack-tip was discretized with a coarser mesh. After some propagation steps and well before the fracture tip moves into the coarse mesh, the fine mesh was shifted near the tip. With the extension of the fracture the discretization of the far field was also extended. The element grading in the original mesh was constructed in such a way that with mesh refinement every element ahead of the tip was subdivided into two elements in the direction of propagation. Figure 4 shows a detail of the mesh near the fracture tip. Uncontrolled increase of the number of elements was avoided by merging two elements into one in the area behind the advancing tip. The information from the old mesh was mapped into the new mesh using higher order interpolation functions. For example, information either was maintained at the common node locations of the old and new meshes or was calculated only at new locations using the 8-node shape functions and appropriate averaging from neighbouring elements. The known shape functions of the 9-node Langragian element have been scaled appropriately and were used to map the information (e.g. stresses) from the old location to the new location of the Gauss points. The efficiency of the remeshing scheme was validated by checking the equilibrium of the external and internal forces immediately after remeshing and before any resolution. The out of balance forces were remarkably found to be of the same magnitude as before remeshing and still smaller than the convergence criterion.

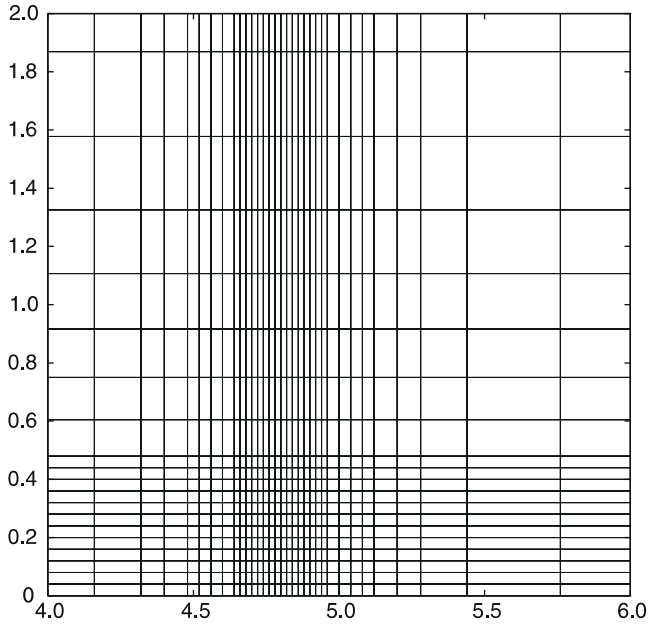

Fig. 4. Mesh detail near the fracture tip

4
Computational results

In this section we present sample results for hydraulically driven fractures in an elastic and an elastoplastic media to show the efficiency of the proposed algorithm. The parameters upon which the numerical computations were based are given in Table 1. The only extra material parameters required for propagating an elastoplastic fracture are the plastic constants. With the chosen material parameters and in situ stresses the rock is initially elastic but very close to a yielding state.

Table 1. Input parameters of computational example

Elastic constants	
Unloading modulus	$E_{\text{unloading}} = 16200\,\text{MPa}$
Poisson ratio	$\nu = 0.3$
Plastic constants	
Friction angle	$\phi = 28^\circ$
Dilation angle	$\psi = 28^\circ$
Initial yield strength	$\sigma_e^0 = 4\,\text{MPa}$
Loading modulus	$E_{\text{loading}} = 1785\,\text{MPa}$
Fracturing parameters	
Fracture toughness	$K_{IC} = 1.0\,\text{MPa}\sqrt{m}$
Uniaxial tensile strength	$\sigma_T = 0.5\,\text{MPa}$
In situ effective stresses	
Vertical stress	$\sigma_3 = 14\,\text{MPa}$
Minimum horizontal stress	$\sigma_1 = 3.7\,\text{MPa}$
Maximum horizontal stress	$\sigma_2 = 9\,\text{MPa}$
Pumping parameters	
Fluid viscosity	$\mu = 10^{-7}\,\text{MPa sec}$
Flow rate	$q_0 = 0.0005\,\text{m}^3/\text{sec m}$

Figure 5 shows the width profile of a propagating fracture in an elastic medium. Allowing for plastic yielding to take place, we obtain the width profile of a propagating elastoplastic fracture shown in Fig. 6. For clarity we plotted the width profile at intervals of every four propagation steps for the elastic fracture and every eight propagation steps for the elastoplastic fracture. The cusping of the crack tips with zero slope is a result of the cohesive model which was incorporated as the propagation criterion. As mentioned earlier, the model of the elastoplastic fracture requires an initial fracture length which was set to 0.5 m; the influence of this can be seen in the width profiles in Fig. 6. If we compare the fracture openings in the region where the fractures were propagated (i.e., distance from wellbore between 0.5 and 2.2 m) we see that the width profile of the elastoplastic fracture is much wider than the width profile of the elastic fracture.

Figure 7 shows the comparison of the net pressure ($p_f + \sigma_1$) profiles in the fracture for the same fracture length. The very narrow opening of the elastic fracture results in greater pressure drop near the fracture tip and significant fluid-lag. Figure 8 compares the net pressures at the wellbore as a function of the fracture length. If this comparison is made over pumping time (as in the field) the required net-pressure for propagating the elastoplastic fracture is much higher than the net-pressure required for propagating the elastic fracture because of the different fracture volumes (Papanastasiou, 1997a).

In order to check the validity of the assumed propagation criterion we plotted in Fig. 9 the stress normal to the propagation direction ahead of the fracture tip. The results show that the tensile stress is contained in a small region near the tip with maximum tensile stress equal to the assumed tensile strength of the weak rock. As

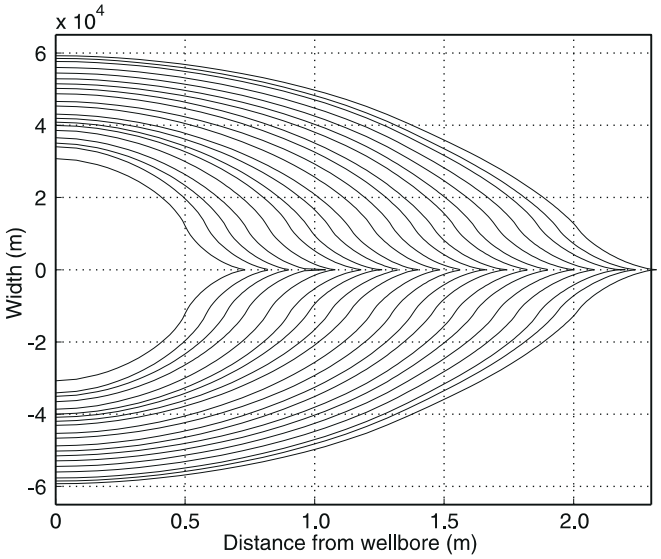

Fig. 5. Width profiles of a propagating elastic fracture

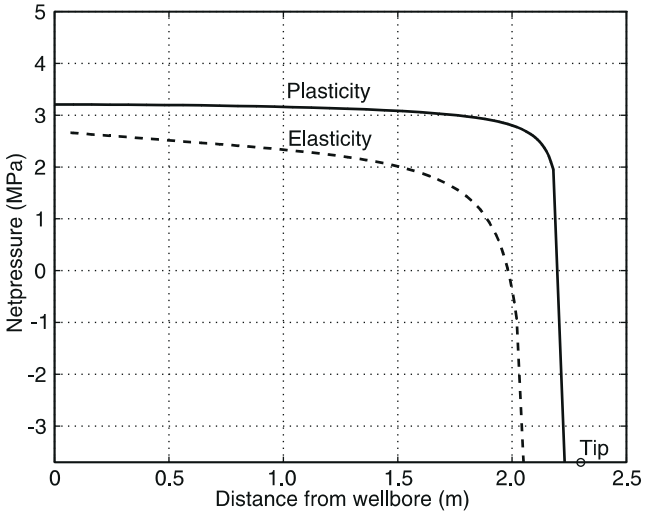

Fig. 7. Net-pressure profiles in the fractures; fracture-tip is shown by 'o'

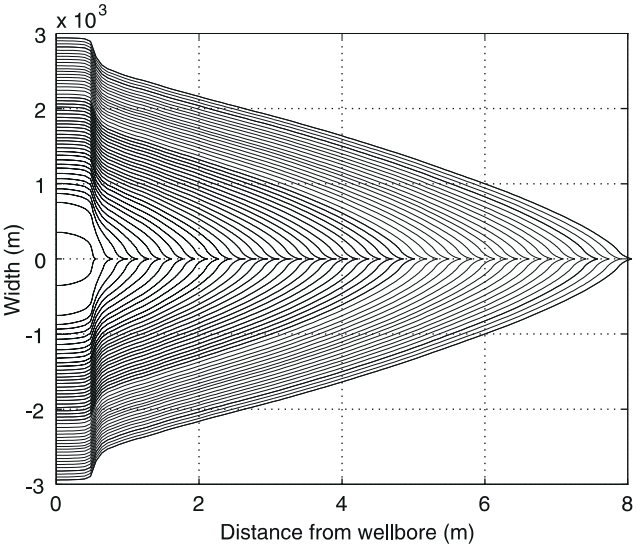

Fig. 6. Width profiles of a propagating elasto-plastic fracture

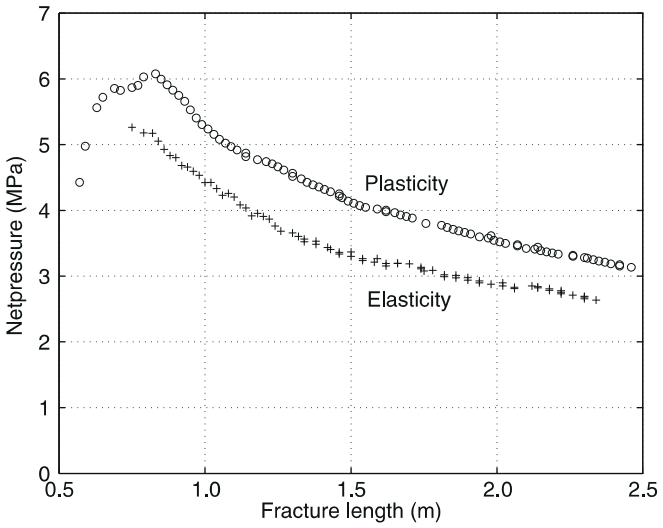

Fig. 8. Net-pressures at wellbore vs fracture length

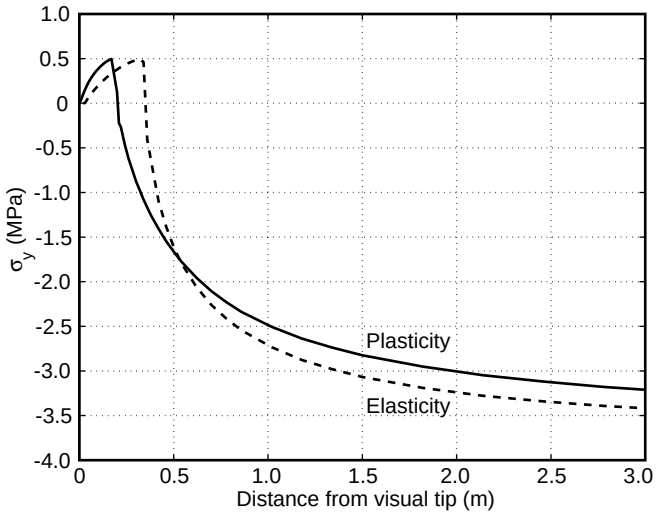

Fig. 9. Profiles of stress normal to the propagation direction ahead of visual tip

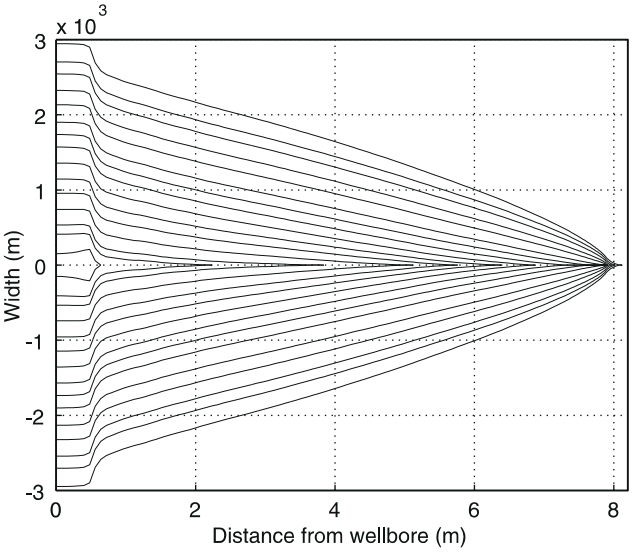

Fig. 11. Width profile of elastoplastic fracture during closure

expected, during the fracturing process there is a relief of the compressive stresses ahead of the fracture tip followed by separation when the normal stress reaches the (very low) tensile strength of the rock. We also observed that the cohesive zone is small for the elastoplastic model and large for the elastic model. This is a result of an extra closing stress imposed from the yielded zone on the propagation line. In addition, we note that although a linear softening constitutive relation was implemented the calculated stress profiles are non-linear. This finding suggests that it is unnecessary to use a more sophisticated softening relation as it requires extra material parameters that are almost impossible to be directly determined in the softening regime.

Plastic yielding near the tip of a propagating fracture provides an effective shielding, resulting in an increase in the effective rock fracture toughness. This is shown in Fig. 10 where we plotted the increase in the effective fracture toughness as a function of the fracture growth.

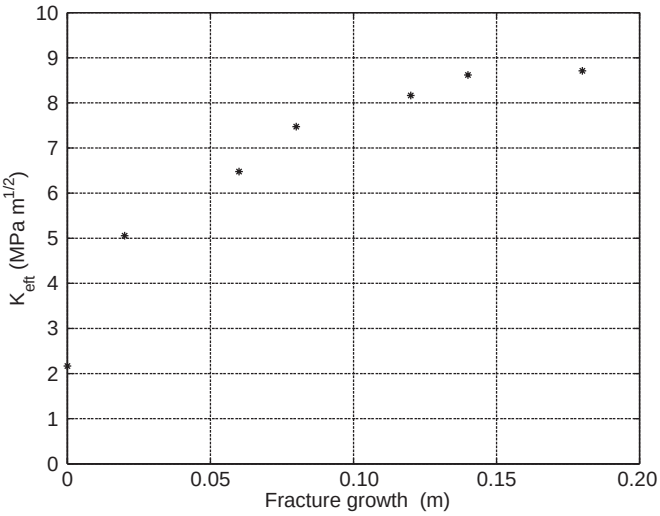

Fig. 10. Effective fracture toughness vs elastoplastic fracture growth

The effective fracture toughness was determined using the calculated, path independent, J-integral (Rice, 1968) according to Eq. (13) with $G_{IC} = J$. The value of the effective fracture toughness is directly related to the size of the plastic zones. After some propagation steps the plastic zones fully develop and the effective fracture toughness reaches an asymptotic value. This asymptotic value can be more than an order of magnitude higher than the original fracture toughness which is determined under lab control conditions. We found that the effective fracture toughness increases with the contrast of the magnitude of the in situ stresses that it is strongly influenced by the strength of the rock and by the elastic modulus but also by the pumping parameters (fluid viscosity and flow rate) (Papanastasiou 1999a).

Finally, in the last computational example we modelled the fracture closure of elastoplastic fracture which has first been propagated. The closing fracture makes surface contact initially near the fracture tip and subsequently towards the mouth of the fracture (Fig. 11). In contrast, a pressurized stationary elastoplastic fracture closes uniformly but remains open after the applied load is released. Practical applications of fracture closure pattern can be found in different aspects of hydraulic fracturing such as in the in situ parameters determination from the inversion of the pressure vs time record and in the closure stress which holds the proppant in place in the fractures (Papanastasiou 1999b, c).

5 Conclusions

In this paper, we presented an efficient algorithm for propagating fluid-driven fractures in pressure sensitive geomaterials. The objective was to study the influence of non-linear rock deformation on propagating hydraulic fractures in order to explain the high net-pressures that are often observed in field operations. Rock was modelled by Mohr-Coulomb flow theory of plasticity for cohesive-frictional dilatent material. Fluid flow was modelled by

lubrication theory. A cohesive crack model which takes into account the softening behaviour of rocks was employed as the propagation criterion. The fully coupled non-linear model was solved numerically by the finite element method. A special continuation method based on the volume of injected fluid in the fracture was used for the direct coupling of the fluid-flow with rock deformation and for controlling the solution during propagation. The efficiency of the proposed algorithm was demonstrated presenting sample results for propagating and receding elastic and elastoplastic fractures.

References

Barenblatt GI (1962) Mathematical theory of equilibrium cracks in brittle fracture. Adv. Appl. Mech. 7:55–129

Barr DT (1991) Leading-Edge Analysis for Correct Simulation of Interface Separation and Hydraulic Fracturing. PhD thesis, MIT

Bazant ZP (1986) Mechanics of Distributed Cracking. Appl. Mech. Review 39(5):675–705

Carbonell R, Detournay E (1999) Self-Similar solution of a fluid-driven fracture in a zero toughness elastic solid. Proc. Royal Society. London Ser. A (submitted)

Carter BJ, Desroches J, Ingraffea AR, Wawrzynek PA (1999) Simulating 3D Hydraulic fracturing. In: Zaman MM, Booker JR, Gioda G (eds), Modelling in Geomechanics, Wiley Publishers (under review)

van Dam DB, de Pater CJ, Romijn R (1997) Experimental study of the impact of plastic rock deformation on hydraulic fracture geometry. Int. J. Rock Mech. Min. Sci. 34: 3–4, paper No. 318

Desroches J, Detournay E, Lenoach B, Papanastasiou P, Pearson JRA, Thiercelin M, Cheng A (1994) The crack tip region in hydraulic fracturing. Proc. Royal Society. London A 447:39–48

Detournay E (1999) Fluid and solid singularities at the tip of a fluid-driven fracture. In: Durban D, Pearson JRA (eds) Proc. IUTAM Symposium on Non-Linear Singularities in Deformation and Flow, 27–42, Dordrecht, Kluwer Academic Publishers

Garagash D, Detournay E (1999) The tip region of a fluid-driven fracture in an elastic medium. J. Appl. Mech. (submitted)

Geertsma J, DeKlerk F (1969) A rapid method of predicting width and extend of hydraulic induced fractures. JPT 21(12):1571–1581

Germanovich LN, Astakhov DK, Shlyapobersky J, Ring LM (1988) A model of hydraulic fracture with Parallel Segments. Proc. Int. Conf. Comp. Eng. Sc., Atlanta, Georgia

GRI (1991) GRI staged field experiment no. 3, Report GRI-91-0048

Hillerborg A, Modeer M, Petersson PE (1976) Analysis of crack formation and crack growth in concrete by means of fracture mechanics and finite elements. Cement and Concrete Research 6:773–782

Johnson E, Cleary MP (1991) Implications of Recent Laboratory Experimental Results for Hydraulic Fractures. Proc. of the Rocky Mountain Regional Meeting and Low-Permeability Reservoirs Symposium, Denver, 413–428

Kanninen MF, Popelar CH (1985) Advanced fracture mechanics. Oxford University Press

Kristianovitch SA, Zheltov YP (1955) Formation of vertical fractures by means of highly viscous fluid. In Proc. 4th World Petroleum Congress, Vol. II, 579–586

Labuz JF, Shah SP, Dowding CH (1985) Experimental analysis of crack propagation in granite. Int. J. Rock Mech. Min. Sci. & Geomech. Abstr. 22:85–98

Papanastasiou P, Thiercelin M (1993) Influence of inelastic rock behaviour in hydraulic fracturing. Int. J. Rock Mech. Min. Sci. &Geomech. Abstr. 30:1241–1247

Papanastasiou P (1997a) The influence of plasticity in hydraulic fracturing. Int. J. Fract. 84:61–79

Papanastasiou P (1997b) A coupled elastoplastic hydraulic fracturing model, Int. J. Rock Mech. Min. Sci. 34:3–4, paper No. 240

Papanastasiou P (1999a) The effective fracture toughness approach in hydraulic fracturing. Int. J. Fract. 96:127–147

Papanastasiou P (1999b) Formation stability after hydraulic fracturing. Int. J. Num. Anal. Meth. Geomech. (in print)

Papanastasiou P (1999c) Hydraulic Fracture closure in a pressure-sensitive elasto-plastic medium. Int. J. Fract. (accepted)

Papanastasiou P, Durban D (1997) Elastoplastic analysis of cylindrical cavity problems in geomaterials. Int. J. Num. Anal. Meth. Geomech. 21:133–149

Ramm E (1981) Strategies for tracing the non-linear response near limit points. In: Wunderlich E, Stein E, Bathe KJ (eds) Nonlinear Finite Element Analysis in Structural Mechanics, Springer-Verlag, Berlin

Rice JR (1968) A path-independent integral and the approximate analysis of strain concentration by notches and cracks. J. Appl. Mech., Trans. ASME 35:379–386

Savitski A, Detournay E (1999) Propagation of a penny-shape hydraulic fracture in an impermeable rock. In: Proc. 37th U.S. Rock Mech. Symp., Balkema Rotterdam

Shlyapobersky J (1985) Energy Analysis of Hydraulic Fracturing, Proc. 26th US Symp. Rock Mechanics, Rapid City, 539–546

Spence DA, Turcotte DL (1985) Magma-driven propagation of cracks J. Geophys. Res. 90:575–580